Distinct cerebellar engrams in short-term and long-term motor learning

Wen Wang[a,b,1], Kazuhiko Nakadate[a,1,2], Miwako Masugi-Tokita[a,1,3], Fumihiro Shutoh[c,1,4], Wajeeha Aziz[a,d], Etsuko Tarusawa[a], Andrea Lorincz[a,5], Elek Molnár[e], Sebnem Kesaf[a,d,f], Yun-Qing Li[b], Yugo Fukazawa[a,d,6], Soichi Nagao[c], and Ryuichi Shigemoto[a,d,f,7]

[a]Division of Cerebral Structure, National Institute for Physiological Sciences, Okazaki 444-8787, Japan; [b]Department of Anatomy, Histology, and Embryology, K. K. Leung Brain Research Centre, Fourth Military Medical University, Xi'an 710032, People's Republic of China; [c]Laboratory for Motor Learning Control, RIKEN Brain Science Institute, Saitama 351-0198, Japan; [d]Department of Physiological Sciences, Graduate University for Advanced Studies (Sokendai), Okazaki 444-8787, Japan; [e]Medical Research Council Centre for Synaptic Plasticity, School of Physiology and Pharmacology, University of Bristol, Bristol BS8 1TD, United Kingdom; and [f]Institute of Science and Technology Austria, 3400 Klosterneuburg, Austria

Edited by Richard L. Huganir, The Johns Hopkins University School of Medicine, Baltimore, MD, and approved November 22, 2013 (received for review August 18, 2013)

Cerebellar motor learning is suggested to be caused by long-term plasticity of excitatory parallel fiber-Purkinje cell (PF–PC) synapses associated with changes in the number of synaptic AMPA-type glutamate receptors (AMPARs). However, whether the AMPARs decrease or increase in individual PF–PC synapses occurs in physiological motor learning and accounts for memory that lasts over days remains elusive. We combined quantitative SDS-digested freeze-fracture replica labeling for AMPAR and physical dissector electron microscopy with a simple model of cerebellar motor learning, adaptation of horizontal optokinetic response (HOKR) in mouse. After 1-h training of HOKR, short-term adaptation (STA) was accompanied with transient decrease in AMPARs by 28% in target PF–PC synapses. STA was well correlated with AMPAR decrease in individual animals and both STA and AMPAR decrease recovered to basal levels within 24 h. Surprisingly, long-term adaptation (LTA) after five consecutive daily trainings of 1-h HOKR did not alter the number of AMPARs in PF–PC synapses but caused gradual and persistent synapse elimination by 45%, with corresponding PC spine loss by the fifth training day. Furthermore, recovery of LTA after 2 wk was well correlated with increase of PF–PC synapses to the control level. Our findings indicate that the AMPARs decrease in PF–PC synapses and the elimination of these synapses are in vivo engrams in short- and long-term motor learning, respectively, showing a unique type of synaptic plasticity that may contribute to memory consolidation.

long-term depression | high-voltage electron microscope | Golgi staining

Image stabilization in the visual field via the vestibulo-ocular reflex and optokinetic response requires accurate extraocular muscle synergies that rely on long-term plastic calibrations in the cerebellar flocculus (FL) and its downstream target vestibular nuclei (VN) (1–8). Long-term depression (LTD) in parallel fiber-Purkinje cell (PF–PC) synapses has been postulated as a possible mechanism for this plastic calibration based on many lines of mutant mice that lack both LTD and learning (9–12). However, LTD's role in motor learning has been recently questioned by a few mutant mice lines (13) and mice with pharmacological treatments (14) that showed lack of LTD but no impairment of learning. Furthermore, long-term potentiation in PF–PC synapses has been also shown to be involved in the motor learning (15). Recent evidence indicates that various forms of synaptic plasticity works synergistically and can compensate each other when one is missing in cerebellar motor learning (16). Despite the apparently contradictory results, no direct evidence for the decrease or increase of synaptic AMPA receptors (AMPARs) has been shown in physiological motor learning. To elucidate in vivo neuronal substrates for motor learning in wild-type mouse, we examined individual PF–PC synapses using quantitative SDS-digested freeze-fracture replica labeling (SDS-FRL) (17) combined with morphometric EM analysis after adaptation of horizontal optokinetic response (HOKR). HOKR is a simple model of cerebellar motor learning and the FL, which is a phylogenetically preserved cerebellar lobule, is involved in the adaptation of HOKR (4, 18). We found that LTD as a form of AMPARs decrease does occur in PF–PC synapses after 1-h training of HOKR. However, LTD lasted less than 24 h, and instead we discovered a drastic elimination of these synapses, which gradually emerged over 5 d of HOKR training. These results indicate distinct engrams in the cerebellum for short-term and long-term memory in motor learning.

Results

Decrease of AMPAR Number After Short-Term Adaptation of HOKR. We used 1-h HOKR training (Fig. S1), performed for five consecutive

Significance

Long-term depression (LTD) of parallel fiber (PF) to Purkinje cell (PC) synapses has been postulated to cause cerebellar motor learning and extensively studied using in vitro preparations. However, there has been no in vivo evidence showing its occurrence after physiological learning, and much controversy on its role has persisted. We demonstrate that LTD as a form of AMPA receptor decrease does occur in PF–PC synapses after adaptation of horizontal optokinetic response. However, it lasted less than a day and was followed by elimination of these synapses. Our findings indicate distinct in vivo engrams for short-term and long-term memory in cerebellar motor learning, and open new mechanistic investigations of how the short-term memory is stabilized through structural reorganization of synaptic connections.

Author contributions: R.S. designed research; W.W., K.N., M.M.-T., F.S., W.A., E.T., A.L., S.K., Y.F., S.N., and R.S. performed research; E.M. contributed new reagents/analytic tools; W.W., K.N., M.M.-T., F.S., W.A., E.T., A.L., Y.-Q.L., Y.F., S.N., and R.S. analyzed data; and W.W., W.A., and R.S. wrote the paper.

The authors declare no conflict of interest.

This article is a PNAS Direct Submission.

Freely available online through the PNAS open access option.

[1]W.W., K.N., M.M.-T., and F.S. contributed equally to this work.

[2]Present address: Department of Basic Biology, Educational and Research Center for Pharmacy, Meiji Pharmaceutical University, Tokyo 204-8588, Japan.

[3]Present address: Department of Anatomy and Neurobiology, Graduate School of Medical Science, Kyoto Prefectural University of Medicine, Kyoto 602-8566, Japan.

[4]Present address: Laboratory of Neuroendocrinology, Graduate School of Comprehensive Human Sciences, University of Tsukuba, Tsukuba, Ibaraki 305-8575, Japan.

[5]Present address: Laboratory of Cellular Neurophysiology, Institute of Experimental Medicine, 1083 Budapest, Hungary.

[6]Present address: Department of Anatomy and Molecular Cell Biology, Graduate School of Medicine, Nagoya University, Nagoya 466-8550, Japan.

[7]To whom correspondence should be addressed. E-mail: ryuichi.shigemoto@ist.ac.at.

This article contains supporting information online at www.pnas.org/lookup/suppl/doi:10.1073/pnas.1315541111/-/DCSupplemental.

days, to induce short-term (STA) and long-term adaptation (LTA). The 5-d HOKR training resulted in varied time courses of gain changes in individual animals (Fig. 1*B*). Some mice developed both STA and LTA, others showed only STA or did not learn at all over the 5 d. However, at population level ($n = 8$ mice), significant but transient daily HOKR gain increases after 1-h training (STA) and gradual but stable increase over 5 d of gain before the daily training (LTA) were observed (Fig. 1 *A* and *C*). First, we measured the density of synaptic AMPARs using SDS-FRL in PF–PC synapses (19) identified with labeling for a mature PF–PC synapse marker, the GluD2 receptor subunit (Fig. 2 *A* and *B*) (20). Mice that developed STA on day (D) 1 showed a decrease (Fig. 2*C*) (Mann–Whitney *U* test, $P < 0.001$) and left-shifted distribution (Fig. 2*D*) (Kolmogorov–Smirnov test, $P = 0.002$) of synaptic AMPAR densities in the FL but not the adjacent paraflocculus (PFL) (Fig. 2 *E* and *F*), which is not involved in HOKR adaptation (1, 21). Pooled data revealed significantly decreased (by 28%) mean density of synaptic AMPARs in the FL (Fig. 2*G*) (Student *t* test, $P = 0.036$ vs. D1 pre) but not the PFL (Fig. 2*G*) after STA on day 1. To confirm that the density changes reflect an altered number of receptors in the target PF–PC synapses, we measured the length of postsynaptic density (PSD) (Fig. 3*A*) and found no changes throughout our experiments. Although previous studies have suggested that GluD2 is closely related to cerebellar motor learning (11), we did not detect changes in GluD2 density in the FL (Fig. 2*G*) after STA. AMPAR reductions varied among individual animals but were well correlated with STA (Fig. 2*H*) (Pearson test, $R = 0.667$, $P = 0.002$). Furthermore, the AMPAR decrease was not observed after 24 h (Fig. 2*I*) ($P > 0.05$, D2 pre vs. D1 post). These results support the idea that LTD caused by the AMPAR decrease in PF–PC synapses is an engram in short-term motor learning in vivo. Decreases in the FL AMPAR density were also observed on day 3 after STA (Fig. 2*I*) (Student *t* test, $P = 0.01$). Interestingly, we could not detect AMPAR decrease after STA on day 5 (Fig. 2*I*) ($P > 0.05$, D5 post vs. D5 pre), which suggests that once LTA is established further STA may be mediated by other mechanisms involving the VN (2, 3) or other regions. Surprisingly, the FL AMPAR densities on day 5 did not differ from that on day 1 pre (Fig. 2*I*) (D1 pre vs. D5 pre, $P = 0.33$; D1 pre vs. D5 post, $P = 0.29$), indicating that AMPAR decrease does not account for LTA.

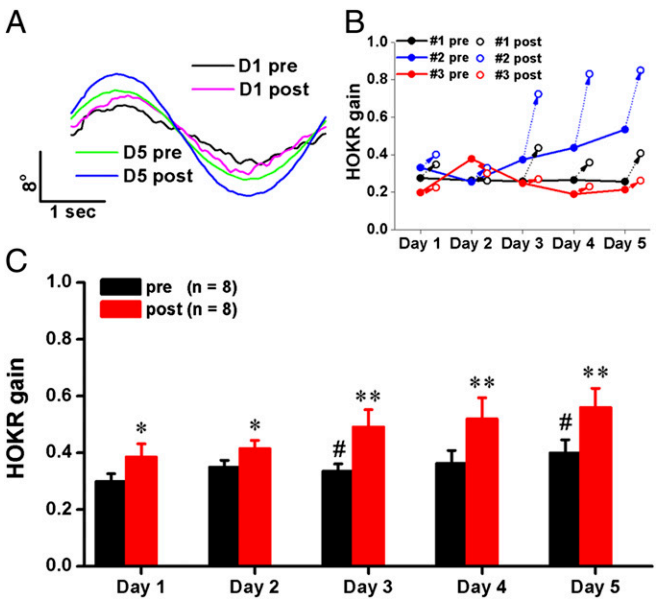

Fig. 1. HOKR training induces short- and long-term adaptation. (*A*) Representative eye-movement traces of a mouse on days 1 (D1) and 5 (D5), before (pre) and after (post) HOKR training. (*B*) Representative learning curves from mice showing only STA (#1, black), both STA and LTA (#2, blue), or no (#3, red) adaptation at all. (*C*) Daily STA was induced by 1-h HOKR training (*$P < 0.05$, **$P < 0.01$, vs. gain measured before the training on each day, paired *t* test) and LTA gradually developed over 5 d of training (#$P < 0.05$ vs. gain measured before the training on day 1, paired *t* test). Data were presented as mean ± SEM.

Elimination of PF–PC Synapses After LTA of HOKR. The net excitatory input to PCs depends not only on the number of postsynaptic AMPARs in individual synapses but also on the number of PF–PC synapses within the target region. Thus, we next analyzed the PF–PC synapse density using the physical dissector method (Fig. S2) and the volume of molecular layer (ML) using serial sections (see Fig. S4) in the FL. The density of the PF–PC synapses did not change after 1-h training on day 1 in either the FL or PFL. However, it was significantly reduced by 33% in the FL but not PFL by day 5 (Fig. 3*B*) ($P < 0.05$). The reduction ratios were similar among the superficial, middle, and deep parts of the ML (Fig. S3). A slight but significant decrease in the volume of ML of the FL was also observed on day 5 ($P = 0.047$) (Fig. 3*C* and Fig. S4). Taking this shrinkage (−18%) into account, the net reduction in PF–PC synapses was about 45%. To further examine the correlation between LTA and the elimination of PF–PC synapses, we measured changes in HOKR gain and synapse density 14 d after the establishment of LTA (Fig. 3*D*). After the animals were kept in normal light-dark cycles without training for 14 d, both HOKR gain and PF–PC synapse density in the FL were not significantly different from the basal levels (Fig. 3*D*, dashed lines). Taken together, these results suggest that the reduction of PF–PC synapses is a reversible structural engram in the LTA of HOKR.

HOKR Adaptation Selectively Involves the Middle FL. It has been demonstrated that PCs in the middle FL (zone 2) along the rostro–caudal axis respond to horizontal movements of the visual field (8, 22) and project to the medial VN (22), which innervates motor nuclei for horizontal eye movement (8). Thus, we restricted our sample selection to the middle one-third (along the medio–lateral axis) of the middle FL (Fig. 3*E*, sections 30–50 of the middle FL). To examine the extent of regions involved in the adaptation of HOKR, we mapped the synapse density in the FL from untrained mice and trained mice on day 5 (Fig. 3 *E*–*G*). We found a prominent reduction in synapse density in the middle but not rostral (zone 3) or caudal (zone 1) FL of trained mice, consistent with the results of functional mapping of PCs involved in the horizontal eye movements (22).

LTA Involves Most PCs Within the Target Region. There is a one-to-one relationship between PF–PC synapses and PC spines (23). Such an arrangement predicts that the synapse elimination in LTA is accompanied by a corresponding PC spine elimination and enables us to examine if most PCs are involved or only a subpopulation of PCs lose more than 33% of synapses. Therefore, we counted the number of spines along individual Golgi-impregnated PC dendritic segments in 3D stereo images from the FL and PFL (Fig. 4*A* and Movie S1). PC dendrites were densely packed with spines in the untrained control animals (~six spines per micrometer of dendritic segment). PC dendrites in the FL but not PFL obtained from LTA mice were covered with significantly less spines (23% reduction, $P < 0.01$) (Fig. 4*B*) than those in the untrained mice. The similar coefficient of variances between the untrained (0.15) and trained FL (0.17) indicated that majority of PCs examined were involved in the spine loss.

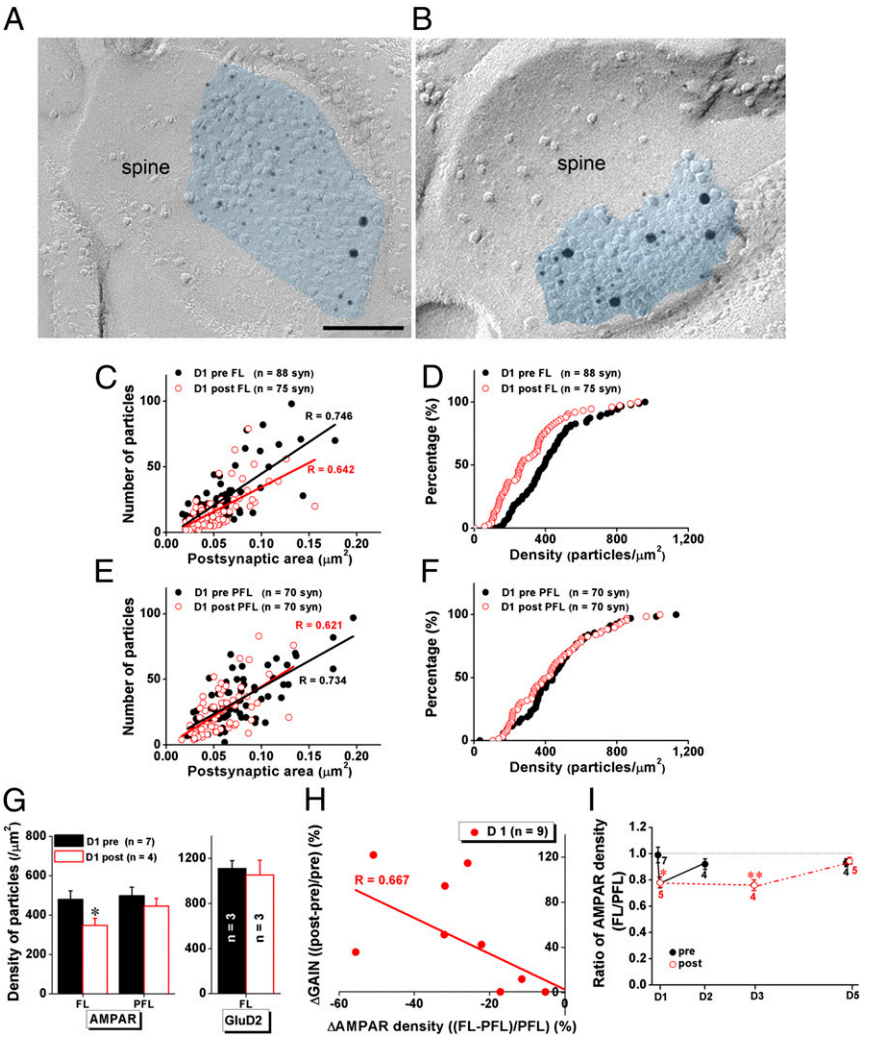

Fig. 2. STA is accompanied with rapid and transient reduction in the density of PF–PC synaptic AMPA receptors selectively in the FL. (*A* and *B*) Labeling for GluD2 subunits (15-nm gold) and AMPARs (5-nm gold) on freeze-fracture replicas from the FL of mice pre- (*A*) and post- (*B*) 1-h training. (Scale bar, 100 nm.) (*C*–*F*) Data from representative mice before and after 1-h training showed that STA was accompanied with decreased synaptic AMPAR density in the FL (*C*) but not PFL (*E*), and left-shifted distribution of AMPAR densities in the FL (*D*, two-sample Kolmogorov–Smirnov test: $z = 1.863$, $P = 0.002$) but not PFL (*F*, $z = 0.930$, $P = 0.353$). The STA did not change the positive correlation between number of AMPARs and size of postsynaptic area (*C* and *E*). (*G*) Pooled data indicated that the STA was accompanied with decreased AMPAR density in the FL ($P = 0.036$) but not PFL. No change in GluD2 receptor density was detected in the FL. (*H*) Data from individual mice at day 1 revealed that the changes in AMPAR density in the FL (normalized to that in the PFL) after 1-h training is negatively correlated with changes in gain (Δgain normalized to pretraining gain, Pearson correlation: $R = 0.667$, $P = 0.002$). (*I*) Density of synaptic AMPARs in the FL significantly decreased after 1-h training on day 1 (D1) and recovered after 24 h (D2). Although density of synaptic AMPARs in the FL also decreased significantly after 1-h training on day 3 (D3), it did not change on day 5 (D5). Black filled circles in *C*–*F* and *I* indicate data obtained before daily training (pre). Red open circles in *C*–*F* and *I* indicate data obtained after daily training (post). Data were presented as mean ± SEM, $*P < 0.05$, $**P < 0.01$ vs. D1 pre, Student *t* test.

Discussion

In this study, we found that the decrease of AMPARs in PF–PC synapses and elimination of these synapses are in vivo engrams in short- and long-term motor learning, respectively. Previous in vitro studies have shown decreases in synaptic AMPAR responses in slice preparations but no structural changes after LTD induction in cultured PCs (24). Other in vivo studies demonstrated PF–PC synaptogenesis induced by learning a complex acrobatic motor skill (25) or PF–PC elimination by eyeblink conditioning (26). In the vestibular ocular reflex (VOR), which shares common output pathways with HOKR (1, 4), gain-decrease but not gain-increase adaptation was improved by estradiol treatment, which also increased PF–PC synapse density (27). In the present study, HOKR gain decrease during the recovery period was accompanied with the increase of synapse density. These results suggest bidirectional and task-dependent structural modifications in cerebellar motor learning.

Despite growing controversies over the role of cerebellar LTD in motor learning (13, 16), we found that the number of synaptic AMPARs does decrease in PF–PC synapses during short-term motor learning, supporting its contribution to motor learning. However, mutant mice with blocked AMPAR internalization showed no deficits in VOR gain-increase and gain-decrease learning despite the lack of LTD (13). The absence of LTD might be compensated by feed-forward inhibition from the ML inhibitory interneurons to PCs (28). Other contributors including long-term potentiation of PF–PC synapses might be also relevant for VOR gain increase and gain decrease (15). Additionally, many types of synaptic and intrinsic plasticity in the cerebellar cortex and its target nuclei have been suggested to contribute synergistically to motor learning in the last decade (6, 16). The

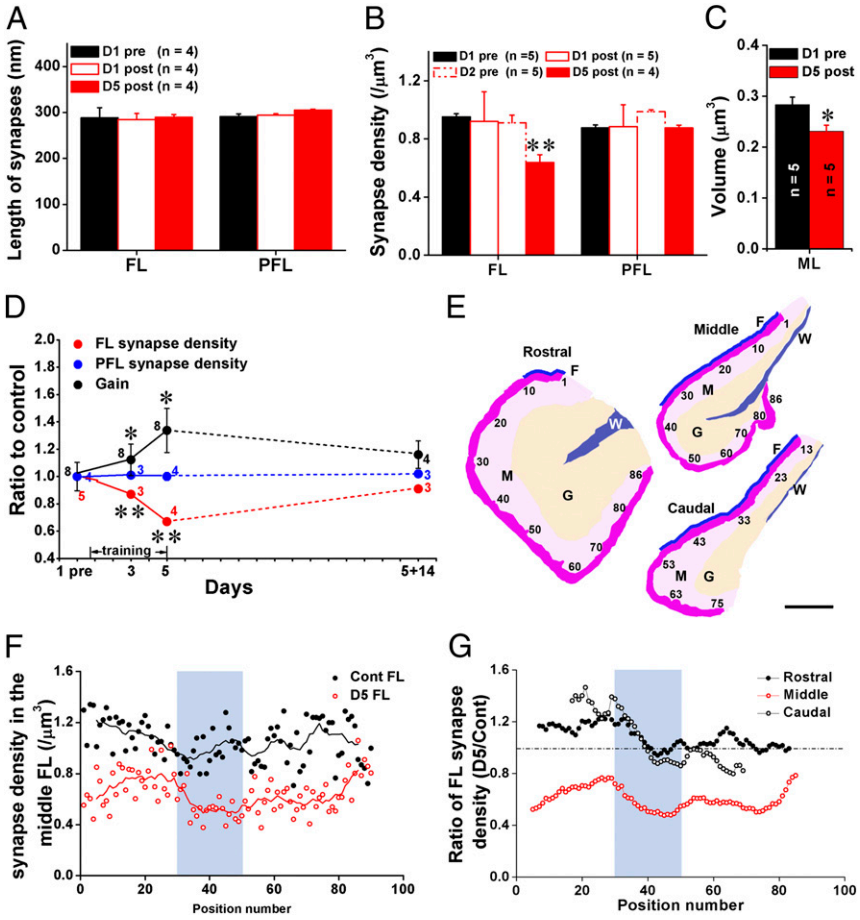

Fig. 3. LTA is accompanied with persistent but reversible elimination of the target PF–PC synapses. (*A*) PF–PC synaptic length was not changed at posttraining on day 1 (D1 post) or 5 (D5 post) compared with basal level (D1 pre) in either the FL or PFL. (*B*) The synaptic density was not changed at posttraining on day 1 (D1 post) or pretraining on day 2 (D2 pre) but decreased by 33% on day 5 (D5 post) compared with D1 pre in the FL. No change was observed in PFL. (*C*) Volume of the molecular layer in the FL was slightly but significantly decreased on day 5 (D5 post) compared with D1 pre. (*D*) Daily HOKR training gradually induced LTA which disappeared after 14 d of light-dark cycle exposure (black circles). PF–PC synaptic density showed correlated reduction in the FL (red circles) throughout this time course. The synaptic density in PFL (blue circles) remained unchanged. HOKR gain is expressed as ratio to control at pretraining. (*E*) Schematic drawing of representative sections of the rostral, middle, and caudal FL showing positions of EM sections used for mapping (shown in *F* and *G*) of synaptic density. The sections were sampled near the surface (dark pink) of the ML (M, light pink). The granule cell layer (G) and white matter (W) are indicated in orange and blue, respectively. Fissure between the FL and PFL is indicated with blue line (*F*). (Scale bar, 200 μm.) (*F* and *G*) Mapping analysis of synaptic density in the FL of control (Cont FL) and 5-d trained (D5 FL) mice showed significant reduction of synaptic density (using corresponding nine adjacent values in two groups, paired *t* test, $P < 0.001$) throughout the medio–lateral extent of the middle but not rostral and caudal FL. Area used for the physical dissector analysis (light blue) showed a prominent reduction in synapse density at D5 compared with control. Data were presented as mean ± SEM, $*P < 0.05$, $**P < 0.01$, vs. D1 pre, Student *t* test.

robust reduction in PF–PC synaptic connections found in our study adds an alternative view to the current integrated multiplasticity model, which includes the transfer of memory traces from the cerebellar cortex to the VN for consolidation (3). The rapid receptor reduction may account for the decreased PC output that drives short-term motor learning. The reduction in PF–PC synapses observed in the LTA phase may play a permissive role to maintain the synaptic plasticity of the VN by persistently reducing PC outputs. Thus, our results suggest that an extensive capacity of the cerebellar cortex with dynamic structural reorganization of synaptic connections underlies long-term memory.

Materials and Methods

Animals. Adult (3-mo-old) male C56BL/6j mice were used in all experiments of the present study. Animal experiments were approved by the animal experiment committee of the National Institute for Physiological Sciences (Okazaki, Japan). All efforts were made to minimize animal suffering and reduce the number of animals used.

Behavioral Experiment. Mice were implanted with a 15-mm–long bolt on the skull with a synthetic resin under isoflurane anesthesia and allowed to recover at least for 24 h. The mouse was mounted on the turntable surrounded by a checked-pattern screen with the head fixed via the bolt, and its body was loosely restrained in a plastic cylinder. The frontal view of the right eye, under the illumination of infrared (wavelength, 860 nm) LED, was captured using a vertically positioned CCD camera (SSC-M350; Sony) and displayed on a 12-inch TV monitor (magnification, 55×). The area of the pupil was determined from the difference in brightness between the pupil and the iris. The real-time position of the eye was measured by calculating the central position of the left and right margins of the pupil at 50 Hz using a position-analyzing system (C-1170; Hamamatsu Photonics) and stored on a personal computer. HOKR was evoked with sinusoidal screen oscillation at 15° and 0.17 Hz (maximum screen velocity, 7.9° per second) in the light, and its gain was defined as the averaged amplitudes of eye movements vs. those of screen oscillation (3). STA was induced by training mice by 1 h of sustained screen oscillation, and LTA by training mice with 1 h of daily sustained screen oscillation successively for up to 5 d. Except for training sessions, mice were kept in dark during LTA. After 5-d LTA, some mice were reared under normal light conditions (12-h light/dark) for 2 wk to extinct LTA.

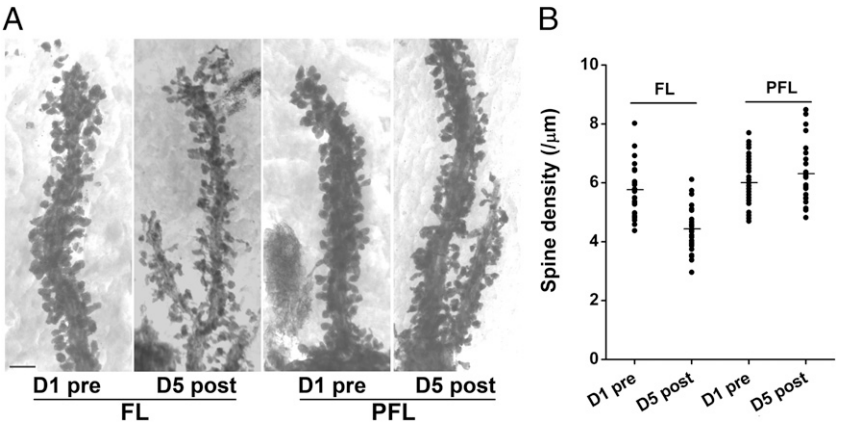

Fig. 4. LTA is accompanied with elimination of PC spines in the FL. (*A*) Representative high-voltage EM images of PC spines along individual dendritic segments in the FL and PFL of control (D1 pre) and trained (D5 post) mice. (Scale bar, 2 μm.) (*B*) Pooled data showed selective spine elimination by 30% in the FL but not in PFL on day 5. Data were presented as mean ± SEM, $^{**}P < 0.01$, vs. D1 pre, Student *t* test.

SDS-FRL. SDS-FRL was performed with some modifications to the original method described by Fujimoto (29) and was used in our previous study (19). Briefly, under sodium pentobarbital (60 mg/kg) anesthesia, mice were perfused through the ascending aorta with 0.5% paraformaldehyde in 0.1 M sodium phosphate buffer (PB). Cerebella (including the FL and PFL) were cut into 120-μm-thick sections with a Microslicer (Dosaka) and cryoprotected with 30% (wt/vol) glycerol in PBS for 12–16 h. The regions including both the FL and PFL were trimmed out, frozen with a high-pressure freezing machine (HPM 010; Bal-Tec) and fractured according to a double-replica method in a freeze-etching system (BAF 060; Bal-Tec). The fractured faces were replicated by carbon (5 nm) with an electron beam gun from overhead and shadowed by platinum/carbon positioned at a 25° angle with rotating (2.5 nm) or at a 45° angle (2 nm) unidirectionally, followed by carbon (20 nm) applied from overhead. The pieces of replica were transferred to 2.5% (wt/vol) SDS containing 0.0625 M Tris and 10% (wt/vol) glycerol, pH 6.8. SDS treatment was performed for 15 min at 105 °C with autoclaving. After the treatment with SDS, replicas were washed with three changes of 0.1% BSA in Tris-buffered saline (TBS) and blocked for 1 h, with two changes of 5% (wt/vol) BSA in TBS. The replicas were then reacted with primary antibodies at room temperature for 1 h, followed by 4 °C for 36–48 h. Double-labeling were performed by using polyclonal rabbit antibody (pan-AMPAR Ab, 3 μg/mL) (30) and polyclonal guinea pig antibody (GluD2 Ab, 0.55 μg/mL). Both antibodies were raised against their specific extraplasmic (E-face) antigen sites. The replicas were then washed three times with 0.1% BSA in TBS, blocked two times with 5% (wt/vol) BSA in TBS for 30 min, and incubated for 1 h at room temperature, followed by 12–16 h at 4 °C or for 2–3 h at 35 °C with the secondary antibodies (1:20 dilution) for goat anti-guinea pig IgG coupled to 15-nm gold particles (GE Healthcare) for GluD2 and goat anti-rabbit IgG coupled to 5-nm gold particles (British Biocell International) for pan-AMPARs in 5% (wt/vol) BSA/TBS. To avoid reciprocal interaction, replicas were first reacted with pan-AMPAR antibody and its secondary antibody followed by incubation in the GluD2 antibody and its secondary antibody. For quantification of GluD2, single-labeling of GluD2 with 5-nm gold particles was used. After immunogold labeling, the replicas were immediately rinsed three times with 0.1% BSA/TBS, washed twice with distilled water, and picked up onto grids coated with pioloform (Agar Scientific).

Quantification of AMPAR and GluD2 Density. Replicas were observed under a Tecnai 12 electron microscope (FEI) and photographed to obtain prints at a magnification of 125,000–213,000×. Immunogold particles were counted in excitatory postsynaptic areas indicated by clusters of intramembrane particles (31, 32). Particles within 30 nm from the edge of synaptic sites were included in the analysis because they can be distant from the epitope (33). The outline of synaptic sites was demarcated free hand along the edge of densely packed intramembrane particles at a distance of <15 nm from each other (Fig. 2 *A* and *B*, blue) (34), and their areas were measured with Scion Image software (Scion). The density of receptors was then defined by the particles per size of the postsynaptic area.

Measurement of Length and Density of Target PF–PC Synapses and Volume of ML. Under sodium pentobarbital (60 mg/kg) anesthesia, mice were perfused through the ascending aorta with 4% (wt/vol) paraformaldehyde, 15% (vol/vol) saturated picric acid, and 0.05% glutaraldehyde in 0.1 M PB. Brains were removed and postfixed in same fixative for overnight at 4 °C, and cut into 50-μm-thick coronal sections on a vibratome (VT 1000S, Leica). Sections containing the whole PFL and FL were mounted on the glass slides and Nissl-stained with Cresyl violet to calculate the volume of the ML. To measure the length and density of target PF–PC synapses, sections were treated with 1% osmium tetroxide, dehydrated, and flat-embedded in epoxy resin (Durcupan ACM, Fluka, Sigma-Aldrich). After being polymerized in a 60 °C oven, blocks were trimmed. A single pair of serial ultrathin sections was cut (Reichert Ultracut S, Leica) at the thickness of 70 nm, collected on piolofrom-coated single-slot grids (Agar Scientific), contrasted by uranyl acetate and lead citrate, and photographed using a JEOL 1200EX electron microscope (JEOL). All analyses were performed in a double-blinded way on electron micrographs. Synapses were defined for the purpose of quantification by the presence of an active zone with clear presynaptic membrane, a postsynaptic membrane with clear PSD, a synaptic cleft, and at least three transmitter vesicles within the presynaptic elements. The size of the synapse was indicated by the measured length of PSD. To obtain a complementary measure of PF–PC synaptic number, unbiased for possible changes in synaptic size, the physical dissector technique (35) was used. The target PF–PC synapses present in the look-up but not adjacent sections were counted. The total number of synapses was summed for at least 40 pairs of electron micrographs and divided by the total volume for each animal as synapse density. To investigate difference in the PF–PC synapse densities along the whole depth of the ML, superficial, middle, or deep regions of the ML of the FL or PFL were analyzed (Fig. S2). For mapping analysis of synaptic density in the FL, we counted the number of PF–PC synapses in single sections (mean area = 330 μm^2) taken from the superficial part of ML along medio-lateral extent of the FL in the middle of rostro–caudal extent. Nine adjacent values shifting from sections 1–9 to 82–90 were used to calculate mean values representing synapse density at the middle positions (each fifth section) in the nine sections.

Spine Density Analysis. To quantitatively analyze the spine density, a rapid Golgi impregnation method was adopted as described previously (36) with some modifications. Under sodium pentobarbital (60 mg/kg) anesthesia, mice were perfused through the ascending aorta with 4% (wt/vol) paraformaldehyde in 0.1 M Millonig's buffer (pH 7.4). The cerebella were dissected and coronal 2- to 3-mm slabs were stored in the same fixative overnight at 4 °C. After washing with 0.1 M cacodylate buffer, the slabs were immersed in a mixture of 2.25% (wt/vol) potassium dichromate and 0.4% osmium tetroxide for 4 d at 20 °C in darkness, and stored in 0.75% silver nitrate solution for 3 d at 20 °C in the dark. After gradual dehydration in alcohol, the tissues were transferred into propylene oxide and embedded in an Epon mixture. Coronol 100-μm sections were made with a vibratome (VT 1000S, Leica) and then re-embedded on glass slides. Five-micrometer sections were made with a Reichert-Jung Ultracut E ultramicrotome (Leica Microsystems), mounted on 75 mesh double-copper grids, and observed under the Hitachi H-1250M high-voltage EM (Hitachi). Pictures were taken under a magnification of 3,000× and at the angles of −8°, 0°, or 8° tilting, respectively. To reconstruct representative 3D movie for each group, serial pictures of an isolated dendritic segment at 3,000× magnification were taken at 2° stepwise tilting, starting from −60° and ending at 60°. Spines along the distal dendritic segment were counted by a blinded

experimenter on the stereo image produced by a pair of 8°-tilted pictures. Spine density was calculated by dividing the number of spines by the length of that segment and was expressed as the number of spines per micrometer (Fig. 4*B*). Seventeen to 56 distal dendritic segments of PCs were randomly selected from the FL or PFL of four individual mice per group.

Quantitative Analysis and Statistics. All of the measurements on pictures were done using a calibration grid (Ted Pella). Scion Image software (Scion) was used to measure synaptic area defined with clusters of intramembrane particle in replica (Fig. 2), the length of target PF–PC synapses (Fig. 3*A*), the length of PC dendritic segments (Fig. 4*B*), the area of region of interest for synaptic density counting, and the volume of the ML (Fig. 3*C*). All data were presented as mean ± SEM. A Student *t* test was used to compare the difference in HOKR gain, synaptic receptor density, length, and density of synapses, density of spine, and volume of the ML. A Pearson test was used to check the correlation between changes in synaptic AMPA receptor density and HOKR gain. A Kolmogorov–Smirnov test was used to check the distribution of densities of synaptic AMPA receptors. For all of the statistical analyses, $P < 0.05$ was considered significant.

ACKNOWLEDGMENTS. We thank T. Arii for the use of the high-voltage electron microscope; and S. Yamada, S. Hara, S. Sawa, and E. Kamiya for technical assistance. This work was supported by Solution-Oriented Research for Science and Technology from the Japan Science and Technology Agency; Ministry of Education, Culture, Sports, Science and Technology of Japan Grant 16300114 (to R.S.); Natural Science Foundation of China Grant 30500278 (to W.W.); Japan Society for the Promotion of Science Fellowship P09125 (to W.W.); a Sasakawa Scientific Research grant from the Japan Science Society (to K.N.); Medical Research Council UK Grant G0601509 (to E.M.); and Biotechnology and Biological Sciences Research Council UK Grants BB/F011326/1 and BB/J015938/1 (to E.M.).

1. Nagao S (1989) Role of cerebellar flocculus in adaptive interaction between optokinetic eye movement response and vestibulo-ocular reflex in pigmented rabbits. *Exp Brain Res* 77(3):541–551.
2. Porrill J, Dean P (2007) Cerebellar motor learning: When is cortical plasticity not enough? *PLOS Comput Biol* 3(10):1935–1950.
3. Shutoh F, Ohki M, Kitazawa H, Itohara S, Nagao S (2006) Memory trace of motor learning shifts transsynaptically from cerebellar cortex to nuclei for consolidation. *Neuroscience* 139(2):767–777.
4. Katoh A, Kitazawa H, Itohara S, Nagao S (1998) Dynamic characteristics and adaptability of mouse vestibulo-ocular and optokinetic response eye movements and the role of the flocculo-olivary system revealed by chemical lesions. *Proc Natl Acad Sci USA* 95(13):7705–7710.
5. Blazquez PM, Davis-Lopez de Carrizosa MA, Heiney SA, Highstein SM (2007) Neuronal substrates of motor learning in the velocity storage generated during optokinetic stimulation in the squirrel monkey. *J Neurophysiol* 97(2):1114–1126.
6. Boyden ES, Katoh A, Raymond JL (2004) Cerebellum-dependent learning: The role of multiple plasticity mechanisms. *Annu Rev Neurosci* 27:581–609.
7. Kitama T, Omata T, Mizukoshi A, Ueno T, Sato Y (1999) Motor dynamics encoding in cat cerebellar flocculus middle zone during optokinetic eye movements. *J Neurophysiol* 82 (5):2235–2248.
8. Nagao S (1988) Behavior of floccular Purkinje cells correlated with adaptation of horizontal optokinetic eye movement response in pigmented rabbits. *Exp Brain Res* 73(3):489–497.
9. Miyata M, et al. (2001) Deficient long-term synaptic depression in the rostral cerebellum correlated with impaired motor learning in phospholipase C beta4 mutant mice. *Eur J Neurosci* 13(10):1945–1954.
10. Shibuki K, et al. (1996) Deficient cerebellar long-term depression, impaired eyeblink conditioning, and normal motor coordination in GFAP mutant mice. *Neuron* 16(3): 587–599.
11. Kashiwabuchi N, et al. (1995) Impairment of motor coordination, Purkinje cell synapse formation, and cerebellar long-term depression in GluR delta 2 mutant mice. *Cell* 81(2):245–252.
12. Aiba A, et al. (1994) Deficient cerebellar long-term depression and impaired motor learning in mGluR1 mutant mice. *Cell* 79(2):377–388.
13. Schonewille M, et al. (2011) Reevaluating the role of LTD in cerebellar motor learning. *Neuron* 70(1):43–50.
14. Welsh JP, et al. (2005) Normal motor learning during pharmacological prevention of Purkinje cell long-term depression. *Proc Natl Acad Sci USA* 102(47):17166–17171.
15. Schonewille M, et al. (2010) Purkinje cell-specific knockout of the protein phosphatase PP2B impairs potentiation and cerebellar motor learning. *Neuron* 67(4):618–628.
16. Gao Z, van Beugen BJ, De Zeeuw CI (2012) Distributed synergistic plasticity and cerebellar learning. *Nat Rev Neurosci* 13(9):619–635.
17. Masugi-Tokita M, Shigemoto R (2007) High-resolution quantitative visualization of glutamate and GABA receptors at central synapses. *Curr Opin Neurobiol* 17(3):387–393.
18. Shutoh F, et al. (2003) Role of protein kinase C family in the cerebellum-dependent adaptive learning of horizontal optokinetic response eye movements in mice. *Eur J Neurosci* 18(1):134–142.
19. Masugi-Tokita M, et al. (2007) Number and density of AMPA receptors in individual synapses in the rat cerebellum as revealed by SDS-digested freeze-fracture replica labeling. *J Neurosci* 27(8):2135–2144.
20. Landsend AS, et al. (1997) Differential localization of delta glutamate receptors in the rat cerebellum: Coexpression with AMPA receptors in parallel fiber-spine synapses and absence from climbing fiber-spine synapses. *J Neurosci* 17(2):834–842.
21. Ito M, Jastreboff PJ, Miyashita Y (1982) Specific effects of unilateral lesions in the flocculus upon eye movements in albino rabbits. *Exp Brain Res* 45(1–2):233–242.
22. Schonewille M, et al. (2006) Zonal organization of the mouse flocculus: Physiology, input, and output. *J Comp Neurol* 497(4):670–682.
23. Napper RM, Harvey RJ (1988) Number of parallel fiber synapses on an individual Purkinje cell in the cerebellum of the rat. *J Comp Neurol* 274(2):168–177.
24. Sdrulla AD, Linden DJ (2007) Double dissociation between long-term depression and dendritic spine morphology in cerebellar Purkinje cells. *Nat Neurosci* 10(5):546–548.
25. Lee KJ, Jung JG, Arii T, Imoto K, Rhyu IJ (2007) Morphological changes in dendritic spines of Purkinje cells associated with motor learning. *Neurobiol Learn Mem* 88(4): 445–450.
26. Connor S, et al. (2009) Eyeblink conditioning leads to fewer synapses in the rabbit cerebellar cortex. *Behav Neurosci* 123(4):856–862.
27. Andreescu CE, et al. (2007) Estradiol improves cerebellar memory formation by activating estrogen receptor beta. *J Neurosci* 27(40):10832–10839.
28. Wulff P, et al. (2009) Synaptic inhibition of Purkinje cells mediates consolidation of vestibulo-cerebellar motor learning. *Nat Neurosci* 12(8):1042–1049.
29. Fujimoto K (1995) Freeze-fracture replica electron microscopy combined with SDS digestion for cytochemical labeling of integral membrane proteins. Application to the immunogold labeling of intercellular junctional complexes. *J Cell Sci* 108(Pt 11): 3443–3449.
30. Nusser Z, et al. (1998) Cell type and pathway dependence of synaptic AMPA receptor number and variability in the hippocampus. *Neuron* 21(3):545–559.
31. Harris KM, Landis DM (1986) Membrane structure at synaptic junctions in area CA1 of the rat hippocampus. *Neuroscience* 19(3):857–872.
32. Landis DM, Reese TS (1974) Differences in membrane structure between excitatory and inhibitory synapses in the cerebellar cortex. *J Comp Neurol* 155(1):93–125.
33. Matsubara A, Laake JH, Davanger S, Usami S, Ottersen OP (1996) Organization of AMPA receptor subunits at a glutamate synapse: A quantitative immunogold analysis of hair cell synapses in the rat organ of Corti. *J Neurosci* 16(14):4457–4467.
34. Tarusawa E, et al. (2009) Input-specific intrasynaptic arrangements of ionotropic glutamate receptors and their impact on postsynaptic responses. *J Neurosci* 29(41): 12896–12908.
35. Sterio DC (1984) The unbiased estimation of number and sizes of arbitrary particles using the disector. *J Microsc* 134(Pt 2):127–136.
36. Browner RH, Baruch A (1982) The cytoarchitecture of the dorsal cochlear nucleus in the 3-month- and 26-month-old C57BL/6 mouse: A Golgi impregnation study. *J Comp Neurol* 211(2):115–138.